Quatrefoil Reentry in Myocardium: An Optical Imaging Study of the Induction Mechanism

SHIEN-FONG LIN, PH.D., BRADLEY J. ROTH,* PH.D.,
and JOHN P. WIKSWO, JR., PH.D.

From the Living State Physics Group, Department of Physics & Astronomy Vanderbilt University, Nashville, Tennessee;
and the *Department of Physics, Oakland University, Rochester, Michigan

Quatrefoil Reentry in Myocardium. *Introduction*: The "critical point hypothesis" for induction of ventricular fibrillation has previously been extended to infer the coexistence of four critical points, and hence four simultaneous spiral reentries or a quatrefoil reentry, resulting from only one premature stimulus delivered to the same location as the pacing stimulus. An optical imaging technique was used to explore its existence and to study the induction mechanism of this peculiar reentry pattern.

Methods and Results : In 16 isolated, Langendorff-perfused rabbit hearts, high-speed optical imaging at 133 or 267 frames/sec was performed to observe the induced response with a unipolar point electrode. A novel quatrefoil-shaped reentry pattern consisting of two pairs of opposing rotors was created by delivering long stimuli during the vulnerable phase. Successful induction occurred in a narrow range of coupling intervals. A dogbone pattern of virtual electrodes was established during the premature stimulus. Propagating wavefronts launched from the virtual anodes immediately after the termination of S2. The alternating blocking and conducting effects of the virtual electrodes, as well as the boundary between virtual cathode and virtual anode, provided the necessary pathways for quatrefoil reentry. Propagation directions of the reentrant spiral wavefronts reversed with a reversal in S2 polarity. Quatrefoil reentries were not sustained and lasted 1 to 4 complete cycles.

Conclusion : The initiation of quatrefoil reentry followed anodal- or cathodal-break stimulation as a result of local symmetrical enhancement of the dispersion of tissue excitability. The "critical point hypothesis" provides the minimum topology required for this type of reentry; the "graded response hypothesis" can be viewed as providing a more detailed explanation of how this topology is actually realized. Triggering mechanisms due to the "break" mode of stimulation also posits a new mechanism for defibrillation. *(J Cardiovasc Electrophysiol, Vol. 10, pp. 574-586, April 1999)*

anisotropy, reentry, spiral wave, intersecting critical contours, bidomain model, cathodal stimulation, anodal stimulation, fluorescence imaging

Introduction

Ventricular fibrillation (VF) can be initiated in normal tissue with an electric shock delivered

Address for correspondence: Shien-Fong Lin, PH.D., Department of Physics & Astronomy, P.O. Box 1807, Station B, Nashville, TN 37235. Fax: 615-322-4977; E-mail: linsf@ctrvax.vanderbilt.edu

during the vulnerable period. During the last decade, systematic studies have led to improved understanding of ventricular vulnerability and also to formulation of a conceptual "critical point" hypothesis.[1,2] The hypothesis states that when the repolarization contour and stimulation contour intersect at a certain "critical point," this critical point becomes a phase singularity point, causing the initiation of a spiral reentry. This hypothesis has been evaluated thoroughly, especially in cases with the pacing electrode and the stimulation electrode placed at different locations on the heart surface.[3,4]

Ventricular reentry can also be induced when the pacing stimulus (S1) and the premature stim-

ulus (S2) are delivered at the same location.[5-8] In this case, the theory may be generalized by taking into account the unequal electrical anisotropies of the intra- and extracellular spaces, resulting in the isostimulus and isorepolarization contours being ellipses with different eccentricities, so that they intersect in four locations and create initial conditions for four simultaneous spiral waves.[2] Chen et al.[3] previously described an observation that closely resembled such a prediction. They found that when S1 and S2 were delivered to the same site, early sites of activation were distributed around all sides of S2. However, the theoretical inference of quatrefoil reentry has never been explored systematically in real hearts, and remains as a missing and intriguing part of the theory of fibrillation.[9]

Recent theoretical studies have provided clues to the mechanisms underlying such an interesting possibility. Numerical simulations[10-12] indicate that when S1 and S2 were delivered at the same site, the hyperpolarization at the virtual anode shortens the refractory period of the S1 wavefront parallel to the fibers, and the depolarization at the virtual cathode lengthens the refractory period of the S1 wavefront perpendicular to the fibers. Thus, a wavefront initiated by the S2 stimulus could propagate parallel to the fibers, but was blocked perpendicular to them. The resulting pair of "arcs of functional conduction block" led to a fourfold symmetric reentrant pattern in their computer model. Most importantly, these studies show that the differing electrical anisotropies of the intra- and extracellular spaces produce large virtual cathodes and virtual anodes that result in differences in the shape of the stimulation and repolarization contours required to support this type of reentry.

In this paper, our goal is to verify, with optical imaging technique, this mechanism of reentry induction in isolated rabbit hearts. Furthermore, we examine both cathodal and anodal S2 stimuli to confirm predicted differences in the reentry pattern with stimulus polarity.

Materials and Methods

Heart Preparation

New Zealand white rabbits, weighing 4.4 to 5.5 kg, were injected with 1,000 units of heparin and 70 mg/kg sodium pentobarbital to induce deep general anesthesia. The heart was excised and the ascending aorta cannulated and secured for retrograde perfusion of the coronaries with a modified HEPES perfusate (108 mM NaCl, 5 mM KCl, 5 mM HEPES, 10 mM glucose, 20 mM $NaC_2H_3O_2$, 1 mM $MgCl_2$, 2.5 mM $CaCl_2$). The perfusate was filtered through a micropore filter, adjusted to pH 7.35 to 7.45 with 1 N NaOH, oxygenated with 100% O_2, and warmed to 37° ± 0.5C. Coronary perfusion pressure was regulated to 80 to 95 mmHg. During the experiment, the hearts were exposed to the air. The calcium channel antagonist D600 was added to the perfusate at a concentration of 1 μM to minimize motion artifacts from the beating heart. The potential-sensitive dye di-4-ANEPPS (Molecular Probes Inc., Eugene, OR, USA) at a concentration of 0.5 μM was added to the perfusate for approximately 15 minutes to stain the heart.

Optical Imaging

Figure 1 shows the setup of the experiment. Fluorescence from the heart surface was elicited by a solid state, frequency doubled laser (Millennia II, Spectra-Physics, Mountain View, CA, USA) at a wavelength of 532 nm. Laser light was delivered to the heart using multiple 1-mm optical fibers (SP-SF-960, FIS Inc., Oriskany, NY, USA), or through a beam splitter and ground glass diffusers to create a double beam illumination scheme.[13] The root mean square variation of laser intensity was 0.1%. The emitting fluorescence was imaged with a high-speed CCD camera (Model CA D1-0256T, Dalsa Inc., Waterloo, ON, Canada) through a color glass with a cutoff wavelength of 590 nm (Schott Glass Technologies, Duryea, PA, USA). The faceplate of the camera was cooled with an ethylene-glycol coolant from a refrigerated waterbath to 15°C. The cooling of the camera reduced the dark current by fourfold to a digitized count of < 100 per pixel for each frame.

Speckle patterns can be seen directly in the laser output or after passing through optical fibers. However, the absorption and scattering of green laser light in cardiac tissue reduced the uneven distribution of induced fluorescence. Because the heart was stationary during imaging, and because the optical transmembrane potential (V_m) was embedded in the variation of fluorescence intensity, the stationary speckle noise did not have a significant effect on the overall signal-to-noise level. In a separate attempt to assess the influence of speckle noise on the quality of flu-
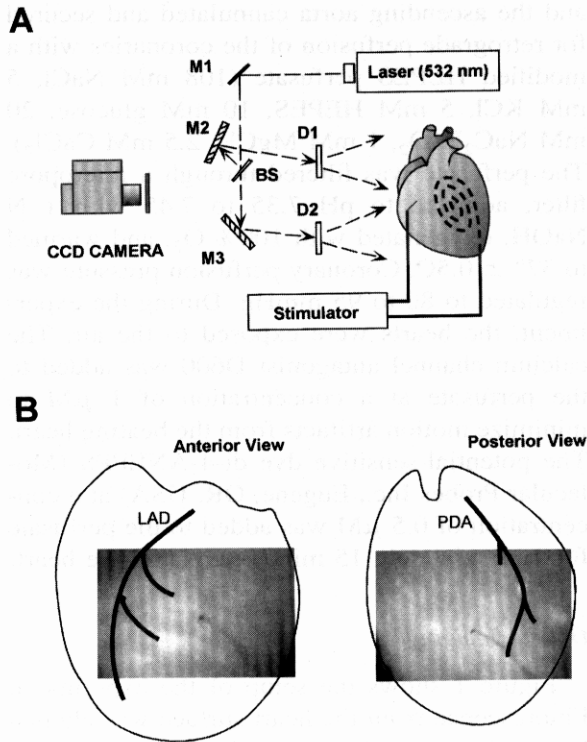
A

B

Figure 1. *(A) A schematic drawing of the experimental setup. A solid-state laser of 532-nm wavelength was used to illuminate the heart through simple optical arrangement, and a CCD camera recorded the fluorescence (M1 to M3: mirrors, BS: beam splitter, D1 and D2: diffusers). Stimuli were applied through a unipolar electrode on the front surface of the heart. A large return electrode (spiral, dashed curve) was placed on the opposite side. (B) Anterior and posterior views of the heart, with the positions of the left anterior descending artery (LAD) and the posterior descending artery (PDA) indicated by the dark curves. The field-of-view of the camera is indicated by the gray scale images superimposed on the outline of the heart.*

orescence recording, the laser diffusers were vibrated at 1 kHz to smooth out laser speckle noise. No difference in the signal-to-noise level was observed as compared to the results obtained with stationary diffusers. Therefore, we concluded that the imaging system sensitivity was limited by the camera noise.

The digitized pixel intensity from the digital camera was transferred to a PCI bus-master frame grabber board (IC-PCI, Imaging Technology Inc., Bedford, MA, USA) that was mounted in an IBM-compatible personal computer (Millennia Pro2 Plus, Micron Computer, Micron Electronics, Nampa, ID, USA). Image acquisition was controlled by Eye Image Calculator (IO

Industries Inc., London, ON, Canada) modified to include external trigger capability.

Experimental Protocol

As shown in Figure 1, a unipolar electrode 0.5 mm in diameter was placed at the center of the frontal or posterior left ventricle, where the muscle fiber orientation was nearly uniform. A spiral silver reference electrode 1 cm in diameter was placed on the opposite side of the heart from the stimulating electrode.

The experiment was performed on 16 hearts. The average weight of the hearts was 19.3 ± 2.6 g. In the first 10 hearts, imaging was performed to visualize the entire anterior view of the heart at 128 x 128 pixels at 133 frames/sec. The purpose of this initial series was to find the appropriate strength interval relationship of S2 and to decide the best electrode locations for the induction of quatrefoil reentry. Imaging procedure for the remaining six hearts was performed at twice the frame rate (267 frames/sec) with an imaging field size of 20.0 x 13.5 mm^2 and an image resolution of 96 x 64 pixels. The higher imaging speed and a close up view of a smaller imaging field allowed more precise determination of spatial temporal information. Therefore, the images presented in this paper were from the high-speed series of the experiment.

The heart was paced with a 2 msec duration electrical stimuli (S1) at two times the diastolic stimulation threshold with a polarity same as the premature S2. To induce reentry, a premature stimulus S2 was delivered following 20 periodic S1 pacing pulses with a cycle length of 500 msec. The premature S2 stimulus, 5 to 40 msec in duration, was applied at an S1-S2 coupling interval of 100 to 180 msec in 10- or 20- msec increments. The strength of S2 was initially set to -20 mA (cathodal stimulation). Once a successful quatrefoil induction was observed, the coupling intervals, S2 strength, S2 duration, and S2 polarity, were altered to observe the difference in the induced responses. In all the induction protocols, the S1 pacing was terminated after the delivery of S2.

Data Analysis

The images, denoted by F_N, were digitized at a resolution of 12-bit/pixel and transferred to a computer for processing. The image processing consisted of first extracting a background image

for diastolic tissue (F_{BG}) from the frame sequence. The variation in the epifluorescence intensity, an indirect estimate of V_m, was then calculated pixel-to-pixel from $-(F_N - F_{BG})/F_{BG}$ for all the frames, producing a frame sequence of V_m, denoted by F_M. The data were then plotted in false colors for visualization.

The fiber direction described in this paper refers to the "apparent fiber direction" defined as the direction of the long axis of the elliptical wavefront elicited by S1 stimulation. The activation isochronal maps were constructed after adaptive Wiener spatial filtering with a neighborhood of 8 x 8 pixels. The nonlinear low-pass filtering process increased the smoothness of the wavefront without altering the activation timing. The spatial resolution of the images after the filtering was estimated to be < 1 mm, appropriate for observation of virtual electrode phenomena which had a size in the range of 4 mm.[14,15] A "difference" sequence (F_D), obtained from subtracting two consecutive F_M images, was used to show the wavefront dynamics with activation isochronal maps. The peak amplitude of action potential elicited by S1 delivered to diastolic tissue was stored in a reference frame, F_{max}. The threshold for determining activation was set to 20% of F_{max}. Therefore, tissue activation was registered when $F_D > 0.2 \ F_{max}$.

Model Simulation

The numerical methods are identical to those presented previously.[12] The tissue is modeled as a 3D bidomain. The conductivities in the intracellular (i) and extracellular (e) spaces parallel to (z) and perpendicular to (r) the fibers are g_{iz} = 0.1863, g_{ir} = 0.0179, g_{ez} = 0.1863, and g_{er} = 0.0894 S/m. The Beeler-Reuter model was used for the active membrane kinetics, modified slightly so that the inward rectifying currents i_{K1} and i_{x1} did not give an unrealistically large membrane conductance for strong hyperpolarization.[12] The electrode was 1 mm long and had a diameter of 0.4 mm. At the outer edge of the tissue (r = 8 mm, z = 20 mm), the intracellular space was sealed and the extracellular space was grounded. The bidomain equations were solved numerically using a space step of 100 μ in the z-direction, and 40 μ in the r-direction, resulting in 201 nodes in each direction. The time step was 10 msec, and the overrelaxation algorithm for computing the extracellular potential was terminated when the largest residual was < 10 μV.

The slow inward current was not blocked or reduced in the calculation.

Results

S2 Response

Excitation in response to S2 could be categorized into "make" or "break" mode of excitation, depending largely on S1-S2 coupling interval (CI).[15,16] Figure 2 shows comparative sequences of tissue response to S1, an S2 at 120 msec CI, and an S2 at 180 msec CI. In Figure 2A, S1 at twice the diastolic threshold elicited an elliptical wavefront. Propagation was fastest in the direction along the line from the upper left to the lower right in each panel. This line was defined as the "apparent fiber direction." In frames 1 to 6 of Figure 2B, a 20 msec/-20mA S2 (cathodal current) was delivered at 120 msec after the onset of S1. A yellow dogbone pattern of V_m depolarization (virtual cathode) was established during S2 with areas of red hyperpolarization (virtual anodes) along the fiber axis. The depolarization and hyperpolarization are used in this paper to indicate relative change in V_m compared to the V_m before S2, instead of comparing to the diastolic V_m. Because the tissue around the electrode had relatively low excitability at this short coupling interval, the depolarized region slowly grew in size with time but did not launch a propagating wavefront. The S2 pulse was terminated after frame 6. In frames 7 to 9, the amplitude of depolarization in the areas transverse to the fiber orientation reduced with time, whereas the hyperpolarized areas in the longitudinal direction started to depolarize, changing from red to yellow. Propagating wavefronts were launched from these hyperpolarized virtual anodes (frames 10 to 12), consistent with cathode-break stimulation. However, the direction of propagation was limited to the fiber direction. Transverse propagation was blocked by the previously depolarized and still recovering virtual cathodes.

In contrast to the break stimulation as shown in Figure 2B, when S2 was delivered at a later time in the refractory period (Fig. 2C, 180-msec coupling interval), the activation sequence more closely resembled S1 stimulation. Activation initially proceeded transverse to the fibers (frames 2 to 4) and did not proceed along the fiber until it has encircled the initially hyperpolarized region
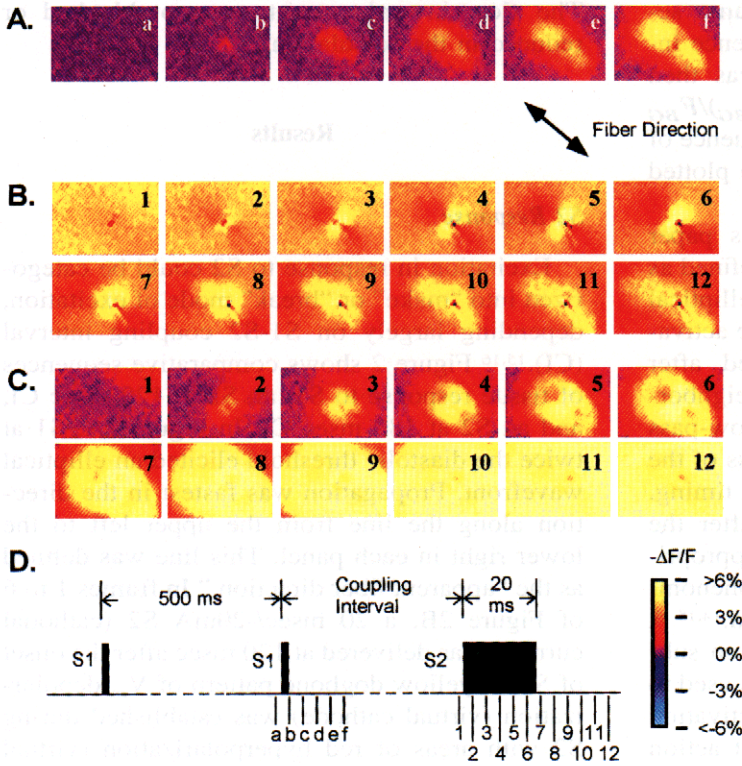
Figure 2. *Images of the transmembrane potential distribution as a function of space and time following an electrical stimulus applied at the center of the tissue. Adjacent frames are separated in time by 3.8 msec, and show a $20 \times 13.5\ mm^2$ area of tissue. The arrow indicates the fiber direction. (A) S1 stimulation (2 mA/2 msec). (B) -20 mA/20 msec S2 stimulus with a coupling interval of 120 msec that produced "break" excitation. The S2 pulse begins in frame 1 and ends in frame 6. (C) -20 mA/20 msec S2 stimulus with a coupling interval of 180 msec that produced "make" excitation. (D) A schematic diagram indicating the stimulation and imaging protocol. The letters and numbers beneath the line correspond to the frames in panels A through C. The colorbar indicates the false-colors for representing the optical transmembrane potential. Yellow is fully depolarized, blue is hyperpolarized, purple is resting.*
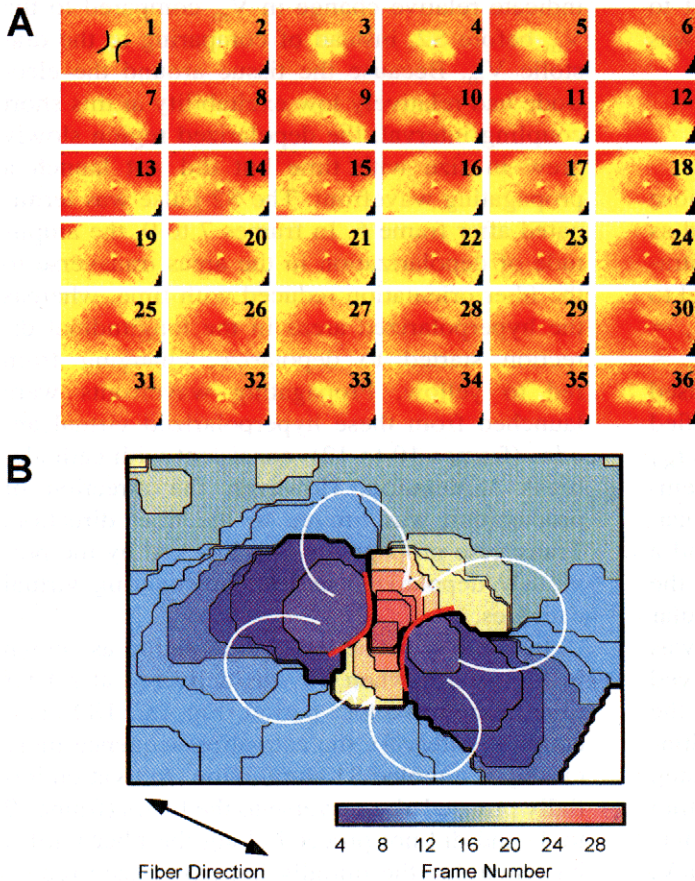

Figure 3. *(A) Images of the transmembrane potential as a function of space and time during cathodally induced quatrefoil reentry. An S2 stimulus (-20 mA, 20 msec) is applied at the center of the tissue; the stimulus ends after frame 1. Smooth curves indicating the borders between the virtual anodes and virtual cathodes are shown in frame 1. B) Pseudocolor isochronal map showing the position of the activation wavefront at subsequent times after the end of the S2 stimulus. The anode-cathode borders in red are superimposed on the activation isochrones to illustrate that these borders formed the arcs of conduction block on the heart surface. Adjacent frames are separated in time by 3.8 msec, and show a $20 \times 13.5\ mm^2$ area of tissue. The arrow indicates the apparent fiber direction.*

of the virtual anodes (frames 4 to 6). Because propagation initiated before the end of the S2 pulse, the mechanism of excitation had switched from "break" to "make."

When the same S2 was delivered very early in the refractory period (< 100-msec coupling interval), a sequence similar to frames 2 to 6 of Figure 2B was observed. However, after the cessation of S2, the clover-leaf shaped charge distribution dissipated passively without inducing a propagating wavefront. This phenomenon was categorized as "no-response" sequences. Thus an S2 delivered at different coupling intervals produced three different sequences: "no response," "break" excitation, and "make" excitation. The "break" mode of S2 stimulation is selected as the primary mode of activation during the experiment because theoretical simulations suggest that "make" stimulations does not induce quatrefoil reentry.[12] Comparing Figures 2B and 2C, we see that tissue response is more homogeneous in the observed field with "make" stimulation than with "break" stimulation, therefore reentry is prohibited under such a condition.

Dynamics of Quatrefoil Reentry

Cathodal stimulation

An episode of quatrefoil reentry induced by cathodal break stimulation is shown in Figure 3A. The 20 msec/-20 mA S2 stimulus was terminated in frame 1. Immediately following the cessation of S2, propagation occurred in the longitudinal direction as charge in the dog-boned-shaped virtual cathode began to diffuse into and excite the adjacent virtual anodes (frame 2). Because of the reduced excitability within the virtual cathodes transverse to the fiber direction, propagation in the transverse direction was blocked. The wavefronts continued to propagate only in the longitudinal direction within the areas under the virtual anodes established by S2 (frames 3 to 9). The wavefronts started transverse propagation after frame 9 moved around the original virtual cathode regions and completely surrounded them in frame 18. The excitability of the virtual cathode recovered during propagation in the outer rims, hence the wavefronts were able to reenter in the transverse direction (frames 21 to 33). However, the propagation was blocked in the longitudinal direction due to earlier depolarization in the virtual an-

odes. The wavefronts from opposite sides of the electrode in the virtual cathodes joined to launch another cycle of the reentrant loop, as demonstrated by the similarity between frames 6 and 36. In this example, a full cycle of quatrefoil reentry went from frame 2 to 32, correponding to a revolution time of 113 msec.

Figure 3B shows an isochronal map constructed from the data in Figure 3A. The thick black lines are the result of nearly superimposed isochrones from multiple frames and show that conduction block follows the borders between the virtual anode and virtual cathode established during the cathodal break stimulus.

The complex dynamics of quatrefoil reentry can be further illustrated with variations in pixel intensity at different locations on the heart. The pixel intensity reveals that the time course of the transmembrane potential differs between specific recording sites. Figure 4 shows the optical V_m obtained from three representative pixels in the transverse direction (V_T), the longitudinal direction (V_L), and the border of the S2-induced hyperpolarized region (V_B). The most obvious criterion to discern the induction of local quatrefoil reentry was a reversal of the relationship in time between V_L and V_T before and after S2. During S1 pacing (time point *a*), V_L preceded V_T due to faster conduction along the fiber axis. After a cathodal S2 that lasted from time *b* to *c*, a reversal of the timing relationship indicated conduction block in V_L and subsequent activation by propagation from V_T, during which V_T (time points *d* and *e*) became activated prior to V_L. V_B, located in the border of virtual electrodes, showed neither depolarization nor hyperpolarization during S2, and exhibited only a small variation in amplitude throughout the two cycles of quatrefoil reentry, apparently due to the wavefront blocking effects as shown in Figure 3. It should be noted that location B was very close to one of the turning points of reentrant wavefront.

Anodal stimulation

An episode of quatrefoil reentry induced by anodal-break stimulation is shown in Figure 5A and follows a sequence that is the perfect complement to the sequence for cathodal-break stimulation in Figure 3A. The 20 msec/30 mA S2 stimulus was terminated in frame 1, in which the hyperpolarized virtual anode (red) has the expected dog-bone shape and the pair of depolarized virtual cathodes are displaced along the fiber
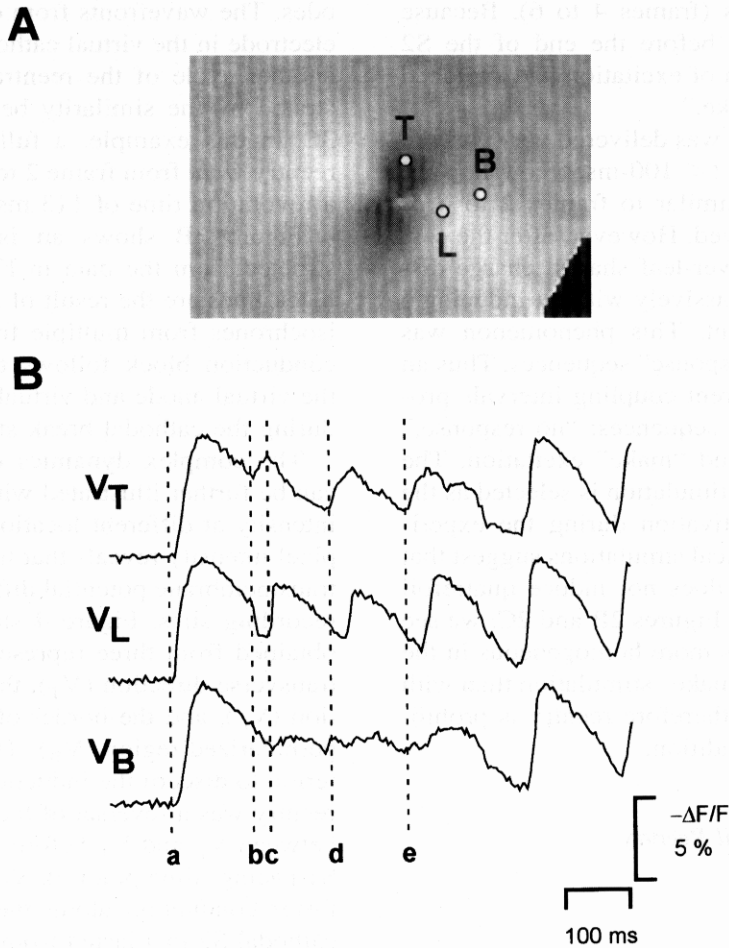
Figure 4. *(A) A gray scale map of the transmembrane potential during the S2 stimulus. Dark is depolarized and light is hyperpolarized, relatively compared to the levels of V_m immediately before S2. (B) The transmembrane potential as a function of time at the three locations marked V_T, V_L, and V_B in A. "a" is the time of the last S1 stimulus, "b" and "c" are the start and end of the S2 stimulus, and "d" and "e" are start times of subsequent depolarizations in the V_T trace.*

direction on either side of the virtual anode. Immediately following the cessation of S2, propagation occurred in the longitudinal direction as charge in the virtual cathode began to diffuse into and excite the narrowest section of the virtual anode (frame 2). Because of the reduced excitability (extended refractoriness) within and beyond the virtual cathodes along the fiber direction, propagation in the longitudinal direction was blocked. In frames 3 to 12, the wavefront continues to propagate only in the transverse direction within the areas under the virtual anodes established by S2. The wavefront started longitudinal propagation only after frame 13, when the wavefront had reached the transverse extent of the original dog-bone shaped virtual anode, moved around the original virtual cathode regions, and completely surrounded them in

frames 19 to 21. The excitability of the virtual cathode recovered during propagation in the outer regions, and hence the wavefronts were eventually able to reenter in the longitudinal direction (frames 22 to 27). However, the propagation was blocked in the transverse direction due to earlier depolarization in the virtual anodes. The wavefronts from opposite sides of the electrode in the virtual cathodes joined to launch another cycle of the reentrant loop, as demonstrated by the similarity between frames 6 and 30, and activation moves in the transverse direction (frames 28 to 36). In this example, a full cycle of quatrefoil reentry went from frame 2 to 27, correponding to a revolution time of 94 msec.

Figure 5B shows an isochronal map constructed from the data in Figure 5A. The thick black lines are the result of the nearly superim-

posed isochrones from multiple frames and show that conduction block follows the borders between the virtual anode and virtual cathodes established during the anodal stimulus. However, the discrepancy between the virtual electrode borders and the lines of conduction block is larger than in Figure 3B. Such a discrepancy may be due to the higher stimulation threshold with anodal current and a lower potential gradient along the boundaries between the virtual electrodes of opposite polarity. The direction of rotation of each of the four reentry pathways (white arrows) is opposite to that for cathodal-break stimulation in Figure 3B.

Comparison of Figures 3B and 5B demonstrates clearly that the anodal-break sequence is the complement to the cathodal-break one, and that in both cases the initial activation is initiated from within the virtual anode (first, purple isochrone) as a result of the substantial charge that has been stored in the adjacent but refractory virtual cathodes and can then diffuse into the virtual anodes. In both sequences, the reentrant circuit is completed (red and dark-red isochrones) by activation of the regions that were initially the virtual cathodes produced by S2. The mechanisms are the same for both cathodal- and anodal-break stimulation, as shown in our earlier studies,[15,16] but the activation patterns reflect the reversal in the locations of the virtual cathodes and the virtual anodes between the two polarities of stimulation. In both Figures 3 and 5, the reentry pathway is determined by the spatial and temporal relationships of the virtual cathodes and anodes.

Inducibility of Quatrefoil Reentry

A total of 35 quatrefoil reentries were induced in the high-resolution series consisting of six hearts. Table 1 summarizes the S2 parameters for the successful quatrefoil induction. The number of quatrefoil reentrant cycles, defined by the simultaneous reentering pair of wavefronts on opposite sides of the stimulating electrode, was mostly in the range of one to two cycles. Quatrefoil reentries lasting more than two cycles were observed in only two occasions with cathodal stimulation. Induction with anodal stimuli appeared more difficult than with cathodal ones, as anodal induction exhibited a wider variation of successful coupling interval (80 to 130 msec) among experiments than cathodal induction (100 to 120 msec). In 27 of the 35 successful inductions, the quatrefoil reentry degenerated into VF. In the remaining eight inductions, the quatrefoil reentry was followed by one to three extra beats and died out.

Due to the strict requirements of electrodynamics for induction of quatrefoil reentries, we investigated further the noninducibility of quatrefoil reentry by altering the coupling interval around the successful ones. For an S1-S2 coupling interval of 20 to 50 msec shorter than the ones of successful induction, the clover-leaf charge distribution remained obvious in the images. After the cessation of S2, such a distribution dissipated passively. When the coupling interval was increased from the successful induction by 10 or 20 msec (n = 10) before entering the region of "make" excitation, the wavefront induced by the break excitation rotated approximately one-quarter to three-quarter cycles along

TABLE 1

Parameters of Premature Stimulus for Successful Quatrefoil Induction, Showing the Range in the Upper Row and Mean ± Standard Deviation in the Lower Row

Cathodal Stimulation (n = 26)				Anodal Stimulation (n = 9)			
Duration (ms)	Strength (mA)	CI (ms)	CL (ms)	Duration (ms)	Strength (mA)	CI (ms)	CL (ms)
10 ~ 40	−10 ~ −40	100 ~ 120	83 ~ 129	20	20 ~ 30	80 ~ 130	83 ~ 125
(20.8 ± 6.3)	(−21.2 ± 6.5)	(115.0 ± 9.9)	(106.3 ± 12.7)		(23.3 ± 5.0)	(111 ± 15.4)	(101.8 ± 13.7)

Number of Quatrefoil Reentrant Cycles	Number of Quatrefoil Reentrant Cycles
1. n = 14	1. n = 6
2. n = 10	2. n = 3
3. n = 1	
4. n = 1	

CI = S1-S2 coupling interval; CL = cycle length of the first cycle of quatrefoil reentries. The range of threshold for diastolic stimulation was 0.3–0.5 mA with cathodal current and 0.7–1.5 mA with anodal current.

the normal quatrefoil pathways, but could not reach the electrode location and faded out. This phenomenon was termed as "nonreentrant break excitation."

Comparison with Modeling Results

Our experimental results are qualitatively similar to predictions based on numerical simulations. Figure 6 shows predictions for cathode-break and anode-break reentry, based on calculations using the bidomain model for the passive electrical properties of the tissue, and the Beeler-Reuter model for the active properties of the membrane. These results are nearly identical to those presented in a previous publication,[12] except that the plot style has been changed to match the style used with the experimental data. A comparison of Figures 3A and 6A (cathode-break stimulation) shows that during the stimulus (frames 1 to 6 in Fig. 3A, t = 300 in Fig. 6A), the tissue is depolarized in a dog-bone shaped region around the electrode, and hyperpolarized along the fiber axis. However, the simulations predict a very strong hyperpolarization near the electrode, where the transmembrane potential drops significantly below its resting level (bright blue). The hyperpolarization was far less pronounced in the experimental data. In both theory and experiment, cathode-break stimulation initiates a wavefront propagating parallel to the fiber axis after termination of the S2 stimulus (frames 7 to 10 in Fig. 3A, t = 320, 340 in Fig. 6A). Subsequently, the wavefront propagates out and around the region directly polarized during the stimulus (frames 15 to 19 in Fig. 3, t = 360 to 380 in Fig. 6A). Finally, the wavefront reenters toward the electrode from both sides, collides near the electrode, and then launches another wavefront parallel to the electrodes (frames 20 to 36 in Fig. 3A; t = 400 to 420 in Fig. 6A). In the simulations, the nonsustained reentrant wavefront died out soon after the t = 420 msec frame in Figure 6A. In the experiment, however, the reentrant activity continued for one to four cycles, and eventually triggered ventricular arrhythmia.

Figure 6B shows the predicted transmembrane potential during anode-break stimulation, which should be compared to the experimental data in Figure 5. Both theory and experiment show a dog-bone shaped area of hyperpolarization during the S2 stimulus, with depolarization along the fiber direction (frame 1 in Fig. 5A; t = 300 in Fig. 6B). Again, the calculations appear to show

a greater hyperpolarization (well below resting potential) than is present in the data. Following the termination of S2, a weak anode-break wavefront propagates away from the electrode in the direction perpendicular to the fibers (frames 2 to 12 in Fig. 5A; t = 320 to 360 in Fig. 6B). This wavefront is slow and weak in both the calculations and the experiment. After the wavefront moves far from the electrode, the wavefront strengthens and begins to encircle the electrode (frames 13 to 18 in Fig. 5A; t = 380 in Fig. 6B). Finally, the wavefront propagates back towards the electrode from both sides along the fiber direction, collides near the electrode, and initiates another wavefront propagating perpendicular to the fiber direction (frames 20 to 30 in Fig. 5A; t = 400 to 420 in Fig. 6B). The reentrant activity lasts for at least one more cycle of the spiral wave in the simulations, and for one or two rotations in the data.

Figure 6C shows isochronal maps of cathodal and anodal reentries predicted by the model. Comparison of the isochronal maps shown in Figures 3B and 5B shows excellent agreement.

Effects of D600

The calcium blocker D600 was used in the experiment to suppress contraction for obtaining satisfactory isochronal maps. D600 could alter the wavefront dynamics to some extent, but should not alter the induction mechanism of reentry. To further test the effect of reduced calcium current on the inducibility of quatrefoil reentry, we performed three additional experiments using DAM (diacetylmonoxime, 15 mM, Sigma Chemical Co., St. Louis, MO, USA) instead of D600 as the electromechanical uncoupling agent. DAM was found to cause a small and reversible reduction of several membrane conductances,[17] and should have less effects on tissue refractoriness than D600. Our results showed qualitative similarities between these two uncoupling agents in the "break" induction mechanism and the conduction pathways. However, the most significant observation in these DAM experiments was an increased coupling interval required for the induction of quatrefoil reentry. The coupling intervals for successful cathodal induction were 140 to 150 msec with DAM, compared to 100 to 120 msec with D600. The shorter S1-S2 coupling interval required for successful induction of quatrefoil reentry is consistent with the hypothesis that 1 μM of D600

Figure 5. *(A) Images of the transmembrane potential as a function of space and time during anodally induced quatrefoil reentry. An S2 stimulus (30 mA/20 msec) is applied at the center of the frame; the stimulus ends after frame 1. Smooth curves indicating the borders between the virtual anodes and virtual cathodes are shown in frame 1. (B) Pseudocolor isochronal map showing the position of the activation wavefront at subsequent times after the end of the S2 stimulus. The anode-cathode borders in red are superimposed on the activation isochrones to illustrate that these borders formed the arcs of conduction block on the heart surface. Adjacent frames are separated in time by 3.8 msec, and show a 20 × 13.5 mm² area of tissue. The arrow indicates the fiber direction.*
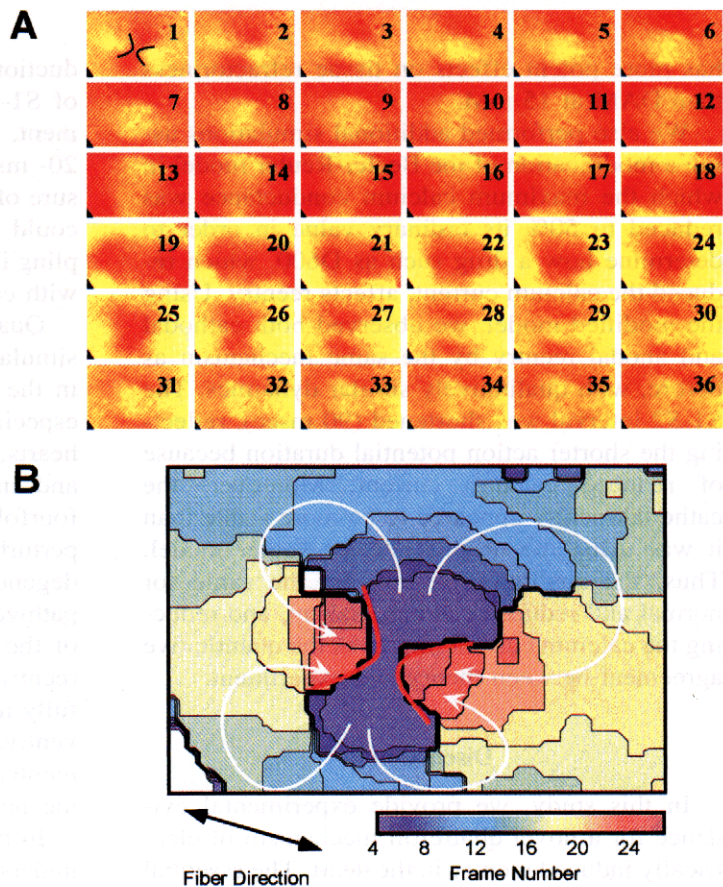
Figure 6. *(A) The theoretical predictions of the transmembrane potential as a function of space and time during cathodally induced (-20 mA/20 msec S2, coupling interval = 280 msec) and (B) anodally induced (25 mA/20 msec S2, coupling interval = 280 msec) quatrefoil reentry, as predicted by a mathematical model. The computational details are described in reference 12. (C) Pseudocolor isochronal maps from the images in A showing the position of the activation wavefront at several times (in msec) after the end of the cathodal and anodal S2 stimulus. The time interval between the subsequent isochrones is 10 msec.*
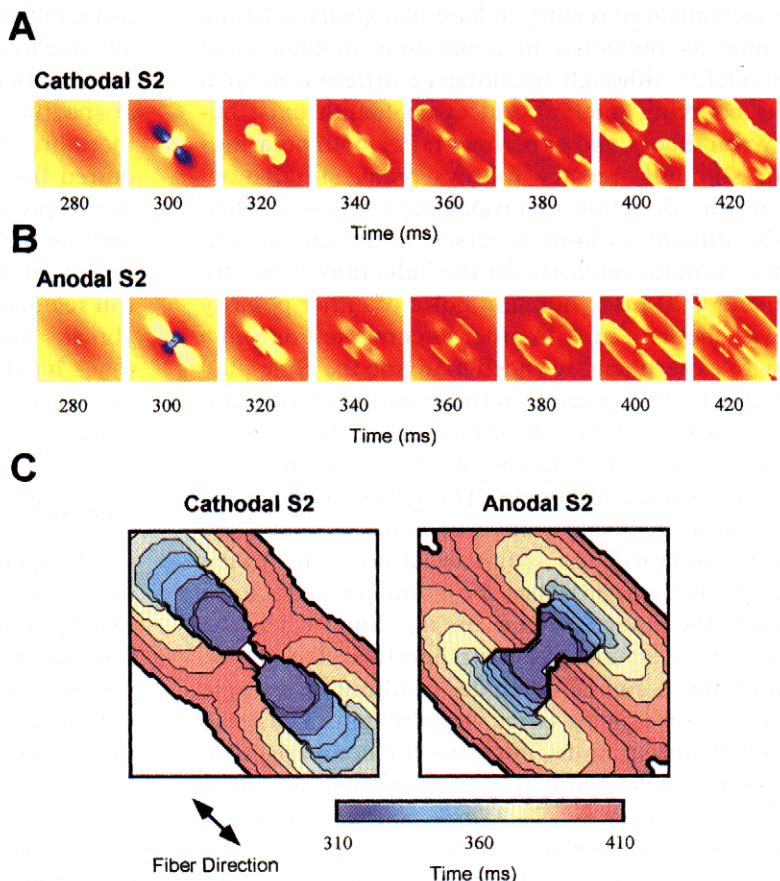
has more potent effects on tissue refractoriness than DAM at 15 mM.

We also performed additional simulations using a modification of the Beeler-Reuter model in which the maximum calcium conductance was reduced to 50% its ordinary value in order to determine how a drug such as D600, which reduced the calcium current, affects reentry. Using the modified model, we observed both cathodal and anodal reentry by the same mechanism as before, with qualitatively similar dynamics. The S1-S2 interval was shortened (90 msec), reflecting the shorter action potential duration because of reduced calcium current. Moreover, the cathodal reentry appeared to be more stable than it was using the original Beeler-Reuter model. Thus, the qualitative results are the same for normal and reduced calcium current, and reducing the calcium current improves the quantitative agreement between theory and experiment.

Discussion

In this study, we provide experimental evidence for a novel quatrefoil mechanism of electrically induced reentry in the heart. The essential mechanism of reentry induction appears to be the same as predicted in a previous mathematical model,[12] although quantitative differences such as coupling interval and cycle length exist between theory and experiment. For both polarities of stimulus, reentry follows break stimulation, and the direction of propagation reverses when the stimulus polarity reverses. In the calculation, the stimulus intensity for the induction of reentry using a 20-msec duration pulse of either polarity was about 14 mA. In order to compare this value with experiment, we need to divide the computed value by two because in the experiment the stimulus was on the heart surface rather than deep in the tissue.[12] The factor of two arises from an image source argument. The tissue-air interface induces an image source of equal strength, the same polarity, and symmetrical position. As the real source approaches the tissue-air surface, so does the image source. In the limit when the source is on the tissue-air interface, the source and image source coincide, resulting in a single source of exactly twice the strength. Thus, the calculated stimulus intensity for comparison to experiment is 7 mA. In the experiment, the mean S2 intensity was -21.2 mA and 23.3 mA for cathodal and anodal induction, respectively. The calculations indicated that quatrefoil reentry in-

duction occurred in a somewhat narrow window of S1-S2 intervals (< 10 msec). In the experiment, the interval was changed in either 10- or 20- msec steps, so we do not have a good measure of the range of intervals over which reentry could be initiated. However, the range of coupling interval data shown in Table 1 is consistent with calculations.

Quatrefoil reentry was not sustained in either simulations or experiment, but persisted longer in the experiments than predicted theoretically, especially for a cathodal stimulus. In rabbit hearts, because of the limited spatial dimension and inhomogeneous fiber-axis orientation, the fourfold symmetry of the reentrant pathway is perturbed and may spontaneously terminate or degenerate into other dominant remote reentry pathways. Furthermore, the intramural rotation of the fiber axis could also disturb stable local reentries.[18] In fact, 77% (27/35) of the successfully induced quatrefoil reentry degenerated into ventricular arrhythmia. Therefore, the quatrefoil reentry may serve better as an VF induction mechanism rather than a sustaining mechanism.

In the present study, our primary goal was to understand the induction mechanism of quatrefoil reentries. Because of the possible tissue damage due to a strong current delivered to the tissue, we did not evaluate the repeatability of induction at specific coupling interval or S2 strength. Furthermore, the variation of the parameters required for induction was not fully characterized in the present study. Instead, the qualitative induction mechanism is firmly established from the results of this study. We concluded that quatrefoil reentries are direct results from a propagated "break" mode of timely tissue activation. On the other hand, the induction failed due to "make" activation or nonpropagating "break" activation from the point current source.

Mechanism of Quatrefoil Reentry

The quatrefoil reentry described in this paper may be viewed as an extreme case of anisotropic reentry that relies on local dual anisotropies to produce the required complexity of activation patterns, and to create symmetrical bands of functional block around the stimulation electrode. These bands of conduction block roughly follow the border of the virtual anodes, exhibit relatively low amplitude of transmembrane potential variation during quatrefoil reentry, and ultimately determine the reentry pathways.

Although this study was motivated by conjectures that followed from the "critical point hypothesis," certain limitations of this hypothesis exist when applied directly to our observations. The clover-leaf shaped virtual electrode pattern produced by the S2 stimulus with either polarity is drastically different from the originally proposed elliptical isostimulus contour.[2] Three different isocontours could be constructed in the peculiar charge distribution topology as shown in Figure 4: isocontours in the virtual cathode, in the virtual anode, and in the boundaries between the virtual cathode and anode. The last one appears to be more appropriate for determining the critical points. Determination of exact positions of critical points is difficult in the present study due to a lack of clear boundaries in the virtual electrode patterns.[15] Unlike induction protocols with different pacing and stimulating sites, the intersection of critical contours cannot be defined precisely, especially for long "break" excitation during which the tissue refractoriness or excitability is continuously modified. By analyzing pixel intensity variations such as those demonstrated in Figure 4, we estimated that the V_m of the turning points where the wavefronts exit the virtual anodes was at 50% to 60% of the peak S1 response.

From the "critical point hypothesis," one would expect to see four concurrent reentrant spiral waves. The morphology of quatrefoil reentrant pathway is clearly different from that of a simple spiral mechanism. As shown in Figures 3, 5, and 6, the wavefront and wavetail are separated by bands of functional block, and the propagation is around an elongated band rather than a core. Alternatively, the wavefront dynamics in quatrefoil reentries may be more appropriately described by the "graded-response hypothesis,"[3,19] which attributes regions of conduction block to graded-response distribution and propagation.

Even so, our results provide reasonable support for the "critical point hypothesis" of induced ventricular reentry. The fact that quatrefoil reentry can only be induced in a narrow window of S1-S2 coupling interval also implies that some critical conditions have to be met for successful induction. The "critical point hypothesis" provides the minimum topology required for this type of reentry; the "graded-response hypothesis" can be viewed as providing a more detailed explanation of how this topology is actually realized. The underlying induction mechanism of quatrefoil reentry emphasizes the importance of fiber orientation and intra- and extracellular anisotropy on electrical induction of VF.

Quatrefoil reentry is a local phenomenon restricted in a region of approximately 20 x 10 mm^2. Figures 3A and 5A show that the outer rim of the wavefront keeps propagating outward while the inner rim is reentering to meet in the center. It is possible that the outer rim of the S2-induced wavefront also create some critical intersections with the gradient of tissue refractoriness. Thus, in addition to the quatrefoil pathways we have described, there could be stronger, but slower competing reentrant pathways coestablished over larger regions of the heart. This may account for some failed induction due to propagation originated outside the imaging field, and could also explain the arrhythmogenetic effect with the "make" excitation in some induction episodes, in which a wavefront of extra beats emerged from elsewhere. We could not verify such a remote mechanism due to the limited size of rabbit hearts. Imaging of larger hearts is necessary to evaluate this remote mechanism.

Implications of Break Excitation

The "break" mode of stimulation has been known for many years,[20,21] however, its mechanism was not unraveled until recently.[15,16] Successful induction of quatrefoil reentries relies on the "break" mode of excitation to enhance the dispersion of local excitability. The polarity of the local transmembrane potential distribution directly adjacent to the electrode is maintained through continuous current injection and charge dissipation during the stimulus. This local "clamping" effect causes the depolarized virtual cathode to become inexcitable, prohibiting propagation of a wavefront through this region following the end of the premature stimulus.

The clamping effect of the "break" pattern was evident in our preliminary search for quatrefoil reentries. We found that break stimulation can occur at an S2 duration as short as 5 msec, or as long as 60 msec. For long S2 pulses lasting 40 to 60 msec, despite the fact that the pulse duration has extended into a region in which "make" excitation would normally take place, we did not observe launching of propagating wavefronts during S2, but, instead, only after the end of S2. During ventricular tachycardia, the dispersion of refractoriness is dynamic. Depending on the shock duration, strength, and tissue refractori-

ness, a defibrillation shock could simultaneously produce "make" and "break" excitations. However, once a "break" pattern is formed, its "clamping" effect would block wavefront movement across the affected area. A reversal of S2 polarity immediately after the "break" pattern could partially or totally offset the charge distribution established previously. This may account for the higher efficacy of biphasic defibrillation shocks.

Limitations

Optical imaging techniques limit the observation to visualizing only the epicardium. The approach cannot reveal the underlying endocardial/ intramural activation and propagation patterns. The 3D reentrant mechanisms through the heart wall remain to be investigated.

References

1. Winfree AT: Electrical instability in cardiac muscle: Phase singularities and rotors. J Theor Biol 1989;138: 353-405.
2. Winfree AT: Ventricular reentry in three dimensions. In Zipes DP, Jalife J, eds. *Cardiac Electrophysiology: From Cell to Bedside.* First Edition. Saunders, Philadelphia, PA, 1990, pp. 224-234.
3. Chen P-S, Cha Y-M, Peters BB, et al: Effects of myocardial fiber orientation on the electrical induction of ventricular fibrillation. Am J Physiol (Heart Circ Physiol) 1993;264:H1760-H1773.
4. Frazier DW, Wolf PD, Wharton JM, et al: Stimulus-induced critical point: Mechanism for electrical initiation of reentry in normal canine myocardium. J Clin Invest 1989;83:1039-1052.
5. Matta RJ, Verrier RL, Lown B: Repetitive extrasystole as an index of vulnerability to ventricular fibrillation. Am J Physiol 1976;230:1469-1473.
6. Shibata N, Chen P-S, Dixon EG, et al: Influence of shock strength and timing on the induction of ventricular arrhythmias in dogs. Am J Physiol 1988;255: H891-H901.
7. Avitall B, Bump TE: Profibrillatory effects of multiple stimuli. J Cardiovasc Electrophysiol 1990;1:197-208.
8. Pertsov AM, Davidenko JM, Salomonsz R, et al: Spiral waves of excitation underlie reentrant activity in isolated cardiac muscle. Circ Res 1993;72:631-650.
9. Winfree AT: How does ventricular tachycardia decay into ventricular fibrillation. In Shenasa M, Borggrefe M, Breithardt G, eds. *Cardiac Mapping* Futura Publishing Co., Inc., Mount Kisco, NY, 1993, pp. 607-623.
10. Roth BJ, Saypol JM: The formation of a reentrant action potential wave front in tissue with unequal anisotropy ratios. Int J Bifur Chaos 1991;1:927-928.
11. Saypol JM, Roth BJ: A mechanism for anisotropic reentry in cardiac muscle. J Cardiovasc Electrophysiol 1992;3:558-566.
12. Roth BJ: Nonsustained reentry following successive stimulation of cardiac tissue through a unipolar electrode. J Cardiovasc Electrophysiol 1997;8:768-778.
13. Lin S-F, Abbas RA, Wikswo JP Jr: High-resolution high-speed synchronous epifluorescence imaging of cardiac activation. Rev Sci Instrum 1997;68:213-217.
14. Wikswo JP Jr, Wisialowski TA, Altemeier WA, et al: Virtual cathode effects during stimulation of cardiac muscle: Two-dimensional in vivo experiments. Circ Res 1991;68:513-530.
15. Wikswo JP Jr, Lin S-F, Abbas RA: Virtual electrodes in cardiac tissue: A common mechanism for anodal and cathodal stimulation. Biophys J 1995;69:2195-2210.
16. Roth BJ: A mathematical model of make and break electrical stimulation of cardiac tissue by a unipolar anode or cathode. IEEE Trans Biomed Eng 1995;42: 1174-1184.
17. Liu Y, Cabo C, Salomonsz R, et al: Effects of diacetyl monoxime on the electrical properties of sheep and guinea pig ventricular muscle. Cardiovasc Res 1993; 27:1991-1997.
18. Panfilov AV, Keener JP: Generation of reentry in anisotropic myocardium. J Cardiovasc Electrophysiol 1993; 4:412-421.
19. Gotoh M, Uchida T, Mandel WJ, et al: Cellular graded responses and ventricular vulnerability to reentry by a premature stimulus in isolated canine ventricle. Circulation 1997;95:2141-2154.
20. Goto M, Brooks C: Membrane excitability of the frog ventricle examined by long pulses. Am J Physiol 1969; 217:1236-1245.
21. Dekker E: Direct current make and break thresholds for pacemaker electrodes on the canine ventricle. Circ Res 1970;27:811-823.